

DOI: 10.36648/2254-609X.9.3.11

Novel Concepts and Materials for Microfluidic Optical Devices

Mitsunori Saito* and Yusuke Itai

Department of Electronics and Informatics, Ryukoku University Seta, Otsu 520-2194, Japan

*Corresponding author: Mitsunori Saito, Department of Electronics and Informatics, Ryukoku University Seta, Otsu 520-2194, Japan, Tel: +815698547233; E-mail: msaito@rins.ryukoku.ac.jp

Received date: June 23, 2020; Accepted date: July 03, 2020; Published date: July 15, 2020

Citation: Saito M, Itai Y (2020) Novel Concepts and Materials for Microfluidic Optical Devices. J Biomedical Sci Vol.9 No.3:11.

Abstract

This article describes recent our experiments that are related to microfluidic optical devices. A biostable phase transition of polyethylene glycol provides novel functions for microfluidic devices. A time-space conversion spectrometry uses a long fluidic cell, for which the microchannel fabrication technique is useful.

Keywords: Microfluidic devices; Polyethylene glycol; Bistability; Fluidic laser; Time-resolved spectroscopy

Introduction

Microfluidic devices have been studied extensively in various technical fields including chemical analyses, biomedical sensing, and optical measurements. A variety of fabrication techniques, measurement methods, and materials have been examined in these two decades [1]. There are still some attractive techniques, however, that will add novel functions to microfluidic devices. This article summarizes our recent experiments that were conducted with fluidic materials.

Polyethylene Glycol

Ethylene glycols (EG and di-EG, tri-EG, or tetra-EG) are used in microfluidic optical devices, since their refractive index is suitable for waveguiding along a channel in a polymer or glass matrix [2]. As **Figure 1a** shows, these molecules are the small version ($m=1-4$) of polyethylene glycol (PEG). PEG types are denoted by using the molecular weight; e.g., PEG 600 ($m=12$). PEGs are useful for creating microfluidic devices due to their non-volatility, non-toxicity, dissolvability for various molecules (bipolarity), and a high index of refraction (1.43-1.46) [3]. They also exhibit a unique thermo-physical feature, i.e., a biostability in the phase transition process. As the photograph in **Figure 1a** shows, PEGs take both a clear liquid phase and a white solid phase at room temperature. **Figure 1b** shows the transmittance change during the heating and cooling processes. A mixture of PEG 300 (95%) and PEG 2000 (5%) exhibits the bistability in the 2C-38C range. Both the sample

heating and cooling can be achieved easily by using a Peltier element. In microdevices, however, a spot control is difficult to achieve with an external heater. To control the phase of each pixel, we created PEG dots that had a self-heating function [4]. Although PEG was an insulator, the electric conductivity could be raised by adding lithium chloride (LiCl, 1.5 mol/l). The conductive PEG dots were sandwiched between two glass plates like a liquid crystal (LC) display. When an alternate voltage (1 kHz, 10 V) was applied between the glass plates, a small Li ion moved back and forth through the network of the solid PEG, and as **Figure 1c** shows, the Joule heating raised the PEG temperature to cause melting.

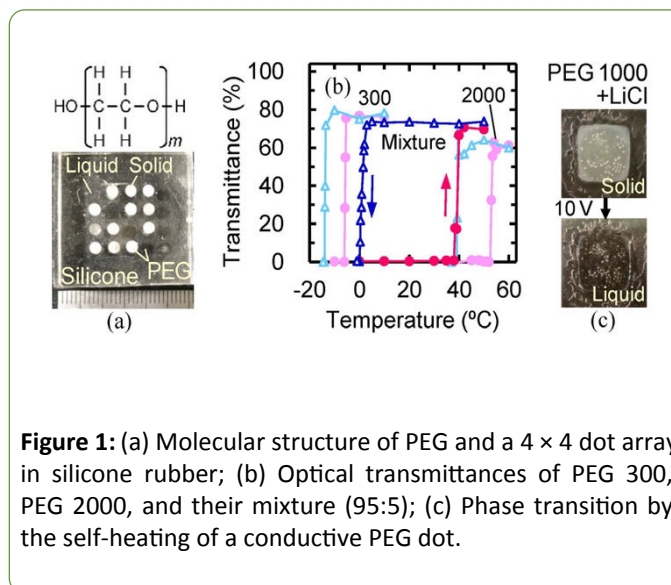


Figure 1: (a) Molecular structure of PEG and a 4 × 4 dot array in silicone rubber; (b) Optical transmittances of PEG 300, PEG 2000, and their mixture (95:5); (c) Phase transition by the self-heating of a conductive PEG dot.

Ring lasers in **Figure 2a** verified the importance of the refractive index in the fluidic channel. When a dye solution (rhodamine 6G, 0.1 mol/l) in the coupled ring channels was excited by a pulsed green laser, only an EG solution exhibited a strong emission at the channel end, as shown in **Figure 2b**. No strong emission was visible with water, since its index (1.33) was smaller than that of the silicone matrix (1.40). The index of glycerol seemed too high to suppress the high-order waveguide modes. **Figure 2c** shows the effect of the ring coupling. As **Figure 2d** shows, the 6-ring system exhibited a laser emission with a threshold of 30 $\mu\text{J}/\text{mm}^2$, while the 3-ring system exhibited a linear growth of the spontaneous emission.

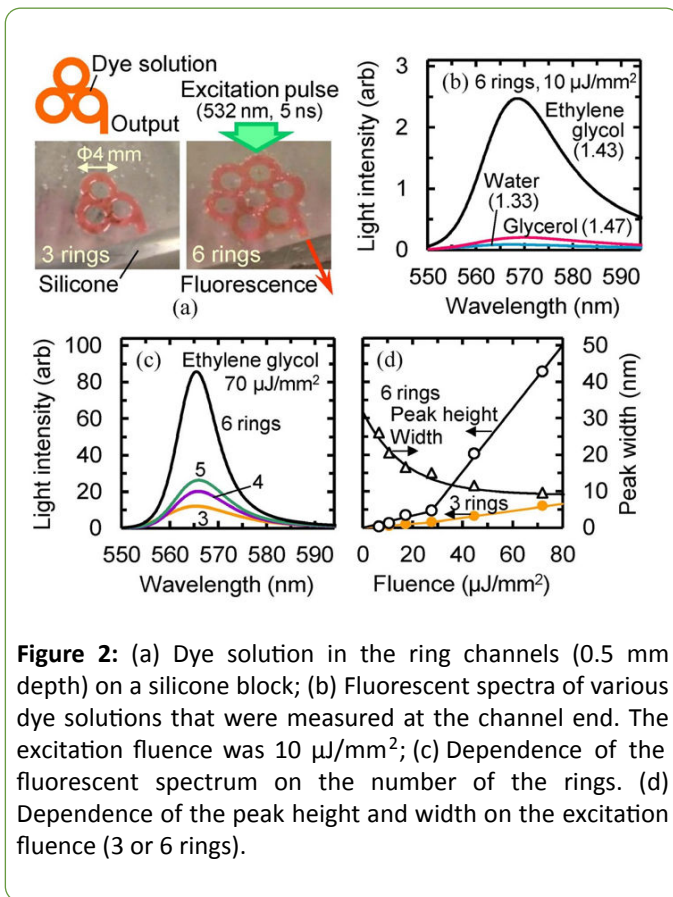


Figure 2: (a) Dye solution in the ring channels (0.5 mm depth) on a silicone block; (b) Fluorescent spectra of various dye solutions that were measured at the channel end. The excitation fluence was $10 \mu\text{J}/\text{mm}^2$; (c) Dependence of the fluorescent spectrum on the number of the rings. (d) Dependence of the peak height and width on the excitation fluence (3 or 6 rings).

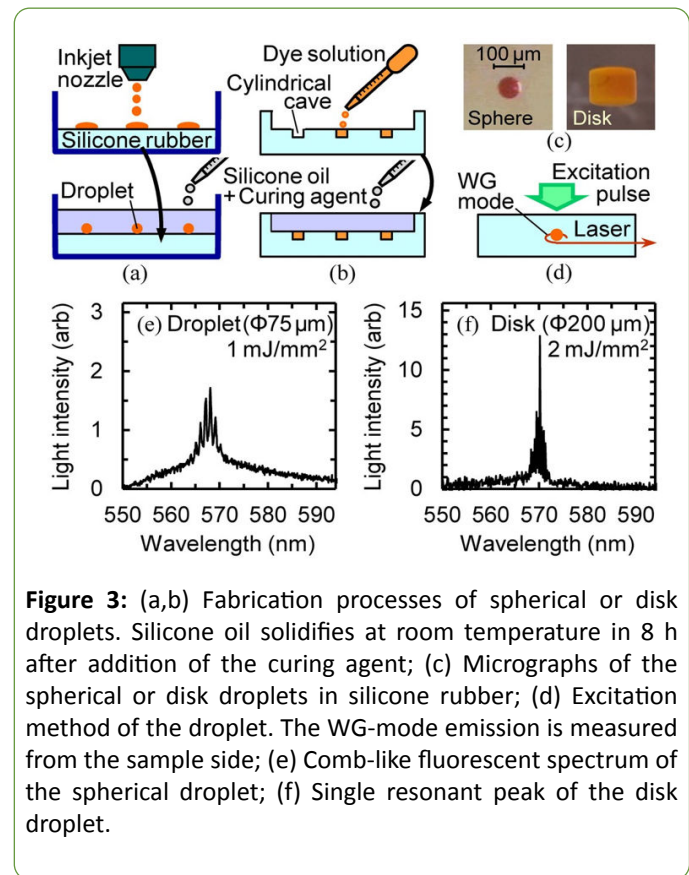


Figure 3: (a,b) Fabrication processes of spherical or disk droplets. Silicone oil solidifies at room temperature in 8 h after addition of the curing agent; (c) Micrographs of the spherical or disk droplets in silicone rubber; (d) Excitation method of the droplet. The WG-mode emission is measured from the sample side; (e) Comb-like fluorescent spectrum of the spherical droplet; (f) Single resonant peak of the disk droplet.

Figure 3a shows the fabrication process of microdroplet lasers. Droplets of dye solution are arranged on silicone rubber by using an inkjet nozzle [5]. When silicone oil is poured on the sample, the droplets take a spherical shape due to the surface tension and are fixed in the rubber after the oil curing process. As **Figure 3b** shows, cylindrical caves have to be prepared in silicone to create disk droplets [6]. **Figure 3c** shows micrographs of the droplets that are enclosed in silicone. As **Figure 3d** shows, the enclosed droplet emits fluorescence when the sample is excited from the top. Since a PEG droplet has a higher index of refraction than the silicone matrix, some fluorescent rays circulate along the periphery; i.e. the whispering gallery (WG) mode is excited. As the light circulates, both a stimulated emission and a resonance take place to create narrow peaks in the fluorescent spectrum. **Figure 3e and 3f** show resonant spectra that were measured with the spherical or disk droplets (WG mode laser). The resonant wavelength is tuneable, since the droplet diameter can be changed by deformation of the silicone rubber [5].

The droplets emit radiation toward various directions as the fluorescent light circulates along the periphery. Experiments have been conducted to extract the WG-mode laser emission at the waveguide end [2,7]. We created a "screw laser" to pick up the WG-mode emission at the helical waveguide end [8]. As **Figure 4a and 4b** show, a PEG solution of rhodamine 6G (103

mol/l) was put into the helical cavity (the inner and outer diameters: 5 mm and 6 mm) that was created with a moulded silicone block and a glass tube. The solution was excited from the inside by irradiating the pulsed laser beam on the inner surface of the glass tube. The fluorescent spectrum was measured at the waveguide end on the silicone surface. As **Figure 4c** shows, the fluorescent peak became narrower as the excitation energy increased, which indicated the occurrence of the stimulated emission.

Adhesive Silicone Sheet

Besides the useful optical properties above, silicone rubber has lots of chemical and mechanical advantages that render it a suitable matrix for creating microfluidic devices. In addition, its adhesiveness provides a simple process for creating liquid-based devices. Modification of silicone molecules raises the adhesion strength notably so that the silicone sheet can be used, for example, to fix a glass panel on smartphones. This strong adhesiveness is useful to construct 3D fluidic channels. As **Figure 5a** shows, we piled adhesive silicone sheets (35 μm thickness, Nippa, NSC-35) alternately with polyester sheets (100 μm thickness). Before piling the sheets, channels and through-holes were created by using a cutting machine (Brother, CMZ102), which had been developed for creating applique (cloth) according to a recorded pattern. A pile of

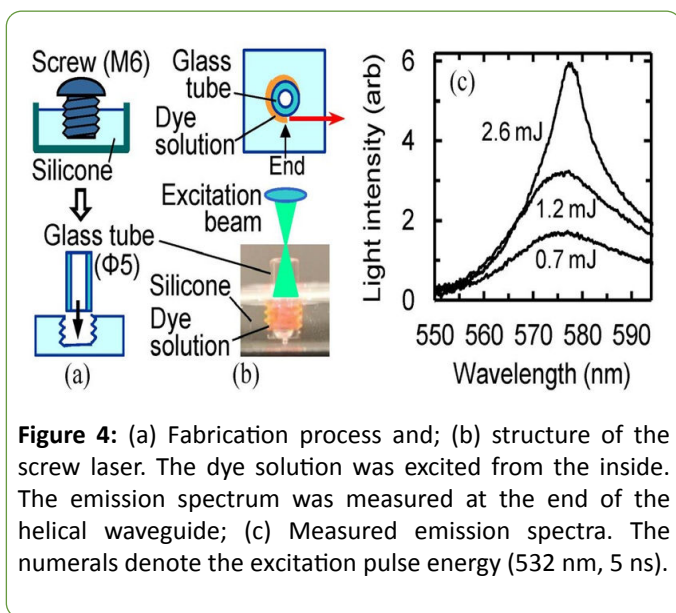


Figure 4: (a) Fabrication process and; (b) structure of the screw laser. The dye solution was excited from the inside. The emission spectrum was measured at the end of the helical waveguide; (c) Measured emission spectra. The numerals denote the excitation pulse energy (532 nm, 5 ns).

these sheets was adhered to a metal plate to create a 3D fluidic channel. The photographs in **Figure 5b** show the flow process. At the start (0 s), water with red pigment entered the nozzle 1, flowed through the fluidic channel, and drained from the nozzle 6. When silicone oil was pushed into the nozzle 2 (1 s), it squeezed in the water flow at the junction. A flexible

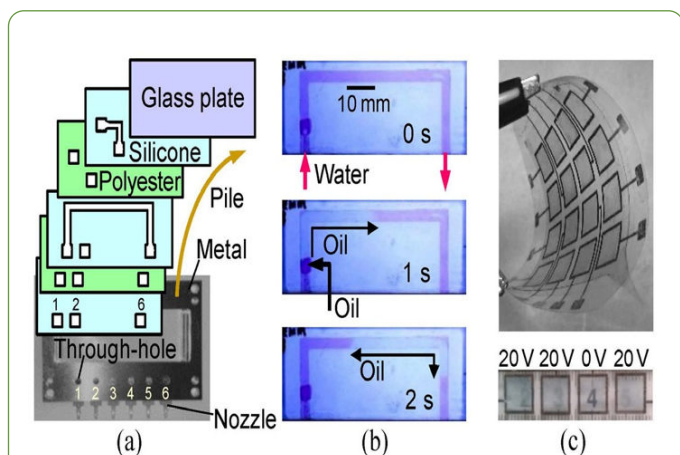


Figure 5: (a) Structure of the 3D fluidic channels. Polymer sheets were piled on a metal plate; (b) Photographs of the sample flow. Water with red pigment entered the channel from the nozzle 1 and flowed out to the nozzle 6. Silicone oil that was momentarily supplied through the nozzle 2 squeezed in the water flow; (c) Flexible pixel array that uses an adhesive silicone sheet to enclose cholesteric LC. Polymer sheets with electrodes and wires were adhered to the silicone sheet. The LC became translucent by the voltage application (20 V).

fluidic device was also fabricated by using the adhesive silicone sheet. **Figure 5c** shows an LC cell array that was fabricated by adhering two polymer sheets (printed wiring) with the silicone sheet. The LC that was enclosed in the opening (cut out) of the silicone sheet exhibited clear or translucent states depending on the applied voltage [9].

Phase Transition of the Fluid

An advantage of the droplet lasers (ring lasers) is their mirror-less structure, which facilitates the microcavity construction. Another method for creating a mirror-less laser is to disperse a fluorescent material in a scattering matrix. As the fluorescent rays are deflected (scattered) repeatedly, they occasionally propagate in a closed path (loop) and induce a stimulated emission like a ring laser. This phenomenon is called “photon localization”, and the resultant strong emission is called “random laser” [10]. Nanoparticles are usually suspended in a dye solution to induce a strong scattering. PEG needs no particles, since it provides a strong scattering in the solid phase, as shown in **Figure 1**. In addition, the laser emission is switchable by the use of the transition between the transparent and scattering phases.

Figure 6a shows emission spectra that were measured with a PEG solution of rhodamine 6G (5×10^{-4} mol/l). The solution was contained in a narrow gap (1 mm) between the ends of two optical fibers (1 mm diameter) [11]. A laser pulse (532 nm, 5 ns, 180 μ J) irradiated the sample top and the emission spectrum was measured through the optical fiber. Although no strong emission was visible in the liquid phase (70°C), a high, narrow spectral peak appeared in the solid phase (30°C). **Figure 6b** shows the dependence of the emission intensity on the excitation energy. When the sample took the liquid phase, the intensity increased in proportion to the excitation energy (the spontaneous emission). In the solid phase, however, the sample exhibited a nonlinear increase with a threshold of 30 μ J, indicating an occurrence of the stimulated emission. In addition, the bistability in the phase transition process caused a bistable laser emission. As **Figure 6c** shows, both the strong and weak emissions were visible at 40°C, when PEG 2000 was mixed with PEG 1000 (20%). **Figure 6d** shows the hysteresis of the emission intensity during the heating and cooling processes.

Inorganic fluorescent materials (phosphors) are used extensively in photonic devices including white LEDs and fiber amplifiers. In comparison with organic dyes, however, the inorganic phosphors generally exhibit a poor excitation efficiency because of a small absorption coefficient. This disadvantage is improved by using PEG as a solvent or a solid matrix for dye dispersion [12].

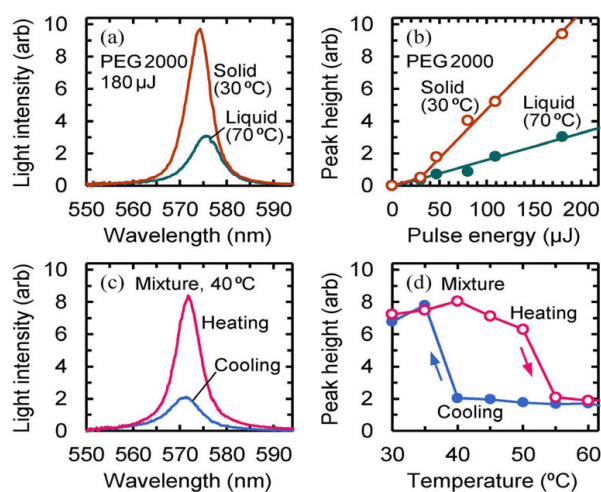


Figure 6: (a) Emission spectra of the PEG solution of rhodamine 6G in the solid or liquid phase; (b) Excitation energy dependence of the spectral peak height; (c) Emission spectra of the PEG mixture (40°C) and (d) the peak height change during the heating and cooling processes (0.1°C/s).

Figure 7a shows fluorescent spectra of an aqueous or PEG solution of europium chloride (EuCl_3 , 0.01 mol/l). The sample solution was contained in a glass cell of 10 mm thickness and excited by a violet laser of 396 nm wavelength (100 mW). The fluorescent peak at 613 nm was 80-fold higher in PEG than water. The reason of the fluorescence enhancement is discussed in Section V. Although the EuCl_3 solution has an absorption band at around the excitation laser wavelength, the absorption coefficient is too low to absorb the laser beam sufficiently; i.e., the solution in the sample cell of 10 mm thickness transmits 95% laser power. The absorption efficiency becomes 1% or less in a thinner sample cell. As the lower spectrum in **Figure 7b** shows, therefore, the fluorescent intensity becomes 1/10 by decreasing the sample thickness from 10 mm to 1 mm.

The weak absorption or the poor excitation efficiency is a serious problem when using the phosphor in microfluidic devices. The scattering in the solid PEG is effective to enhance the excitation efficiency, as shown by the upper spectrum in **Figure 7b**. PEG 1000 was heated to 70°C to dissolve EuCl_3 , since it took the solid phase below 40°C. As the solution was cooled to room temperature, the fluorescence became stronger due to the increase in the scattering strength. It is predicted that the scattering strength increases by mixing several PEGs with different molecular weights. A mixture with a stronger scattering will possibly confine the excitation light in a small sample to attain the complete absorption.

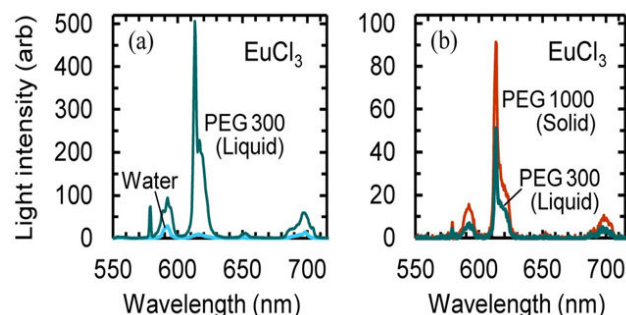


Figure 7: (a) Fluorescent spectra of an aqueous or PEG solution of EuCl_3 (0.01 mol/l). The sample thickness was 10 mm; (b) Fluorescent spectra of the liquid and solid PEG solutions of EuCl_3 . Sample thickness was 1 mm.

Spectrometry of Fluidic Samples

Spectrometry is an important tool for chemical or biomedical analyses including microfluidic sensor technology. Recent progress in the fast-response instruments, e.g. pulsed lasers and image intensifiers, has promoted a development of time-resolved spectrometers. Microfluidic devices seem to play an important role in the fast-response sensors [13]. The time-resolved measurements are usually conducted by using a pulsed laser, i.e. a femto-second, pico-second, or nano-second laser, which is both expensive and difficult to operate. A flow in the fluidic channel is useful to conduct time-resolved measurements that need no pulsed lasers [14,15].

We developed a spectrometer that can measure the photoluminescence spectra with a temporal resolution of nano-second or micro-seconds [16,17]. This spectrometer consisted of slow devices, i.e. a continuous-wave laser diode (LD) and a CCD based spectrometer. **Figure 8a** shows the measurement principle (the time-space conversion method). An excitation beam of an LD (396 nm) is swept by a polygon mirror (500 revolutions/s) or a Galvano-mirror (30 Hz). The beam moves across a long sample cell (or fluidic channel) to excite a fluorescent solution in it. First ($t=0$), a point A is excited and emits fluorescence, which is reflected by the mirror and imaged at a point Q on the confocal plane (the solid line). The adjacent point P receives no fluorescence, since the corresponding point B is not excited. After a time, passage ($t=\Delta t$), the mirror rotation swings the laser beam to excite B (the dotted line), and at the same time changes the correspondence of the image points, i.e., $A \leftrightarrow R$ and $B \leftrightarrow Q$. It

follows that Q receives a fluorescence of the irradiated point B, and R receives an afterglow at A. Further, at $t=2\Delta t$, the laser beam irradiates the point C, and the image correspondence changes to $A\leftrightarrow S$, $B\leftrightarrow R$, and $C\leftrightarrow Q$. In this manner, Q always receives the fluorescence of the irradiation point or the excitation moment. On the other hand, R and S receive the afterglow with a delay of Δt or $2\Delta t$, respectively.

We measured the fluorescent spectra by moving the probe fiber of a multi-channel spectrometer on the image plane (\rightarrow) to attain a series of time-resolved spectra. **Figure 8b** shows the temporal change of the spectral peak height that was measured for the solutions of **Figure 7a**. These times resolved measurements revealed that the fluorescence enhancement in PEG was caused by the extension of the lifetime (τ) of the emission level [16]. **Figure 8c** shows the spectral change of an organic dye (Central Techno, Lumisis® B-800), which demonstrated the capability of the time resolved measurements in the nano-second range.

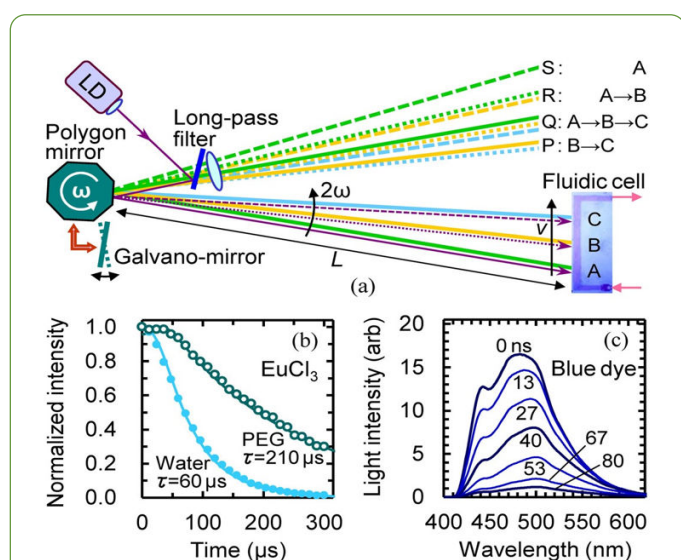


Figure 8: (a) Principle of the time-space conversion spectrometry. A spinning polygon mirror or a swinging Galvano-mirror sweeps both the excitation beam and the fluorescent rays. The solid, dotted, and dashed lines denote the sequence of the optical path change. The sample is a fluorescent solution in a 3+ glass cell or a fluidic channel; (b) Fluorescence decay (613 nm) of the Eu ions in water or PEG 300, i.e., the same solutions as the samples of **Figure 7a**. These measurements in the micro-second range were conducted by using a Galvano-mirror; (c) Spectral change in the decay process of an organic blue dye in PEG 600 (liquid). These measurements in the nano-second range were conducted by using a polygon mirror.

Summary

The bistability is a unique feature of PEG, which will extend the performance of microfluidic devices; e.g., a sample flow can be paused for measurement by freezing the solution. The adhesive silicone sheet is useful to create flexible devices in a simple process. A microfluidic channel provides a suitable sample cell for the time-resolved fluorescent spectrometry that needs a long solution to achieve a sensitive measurement.

Conflict of Interests

The authors have no conflict of interests to declare.

References

- Giri B (2017) Laboratory Methods in Microfluidics. Elsevier 1st Ed: 178.
- Lee W, Li H, Suter JD, Reddy K, Sun Y, et al. (2011) Tunable single mode lasing from an on-chip optofluidic ring resonator laser. Appl Phys Lett 98: 061103.
- Rbeiro P, Andrews DL, Raposo M (2019) Optics, photonics and laser technology. Springer 222: 99-117.
- Saito M, Tsuji K (2018) Bistable optical functions of polyethylene glycol. Proceedings of 2nd IEEE International Conference on Dielectrics, Budapest, 33.
- Saito M, Koyama K (2010) Deformable microdroplet cavity fabricated by an inkjet method. Jpn J Appl Phys 49: 092501.
- Saito M, Hashimoto T, Taniguchi J (2017) Fabrication of disk droplets and evaluation of their lasing action. Opt Lett 42: 4119-4122.
- Linslal CL, Mathew S, Radhakrishnan P, Nampoori VPN, Girijavallabhan CP, et al. (2013) Laser emission from the whispering gallery modes of a graded index fiber. Opt Lett 38: 3261-3263.
- Sumetsky M (2005) Uniform coil optical resonator and waveguide: transmission spectrum, eigenmodes, and dispersion relation. Opt Express 13: 4331-4340.
- Saito M, Uemi H (2016) A spatial light modulator that uses scattering in a cholesteric liquid crystal. Rev Sci Instrum 87: 033102.
- Wiersma DS, Albada MP, Lagendijk A, Lawandy NM, Balachandran RM (1995) Random Laser? Nature 373: 203-204.
- Saito M, Nishimura Y (2016) Bistable random laser that uses a phase transition of polyethylene glycol. Appl Phys Lett 106: 131107.
- Saito M, Koketsu T (2018) Fluorescence enhancement of a bleach resistant solution for use in microfluidic devices. Opt Mater Express 8: 676-683.
- Ugawa M, Lei C, Nozawa T, Ideguchi T, Carlo D, et al. (2015) High-throughput optofluidic particle profiling with morphological and chemical specificity. Opt Lett 40: 4803-4806.
- Kaun N, Vellekoop MJ, Lendl B (2006) Time-resolved Fourier transform infrared spectroscopy of chemical reactions in solution using a focal plane array detector. Appl Spectrosc 60: 1273-1278.

15. Saito M, Okubo Y (2007) Time-resolved infrared spectrometry with a focal plane array and a Galvano-mirror. *Opt Lett* 32: 1656-1658.
16. Saito M, Koketsu T, Itai Y (2019) Time-space conversion for time resolved spectroscopy. *OSA Continuum* 2: 726-1733.
17. Saito M, Itai Y (2020) Time-space conversion spectral analysis for the nanosecond fluorescent processes of organic-inorganic compounds. *AIP Adv* 10.